ACS APPLIED MATERIALS & INTERFACES

Research Article

www.acsami.org

New Insight into Copper Sulfide Electrocatalysts for Quantum Dot-Sensitized Solar Cells: Composition-Dependent Electrocatalytic Activity and Stability

Chung Soo Kim,[†] Sun Hee Choi,[‡] and Jin Ho Bang*[,†,§]

[†]Department of Bionanotechnology and [§]Department of Chemistry and Applied Chemistry, Hanyang University, Ansan, Kyeonggi-do 426-791, Republic of Korea

[‡]Pohang Accelerator Laboratory (PAL), Pohang University of Science and Technology (POSTECH), Pohang, North Gyeongsang Province 790-784, Republic of Korea

Supporting Information

ABSTRACT: Despite recent significant strides in understanding various processes in quantum dot-sensitized solar cells (QDSSCs), little is known about the intrinsic electrocatalytic properties of copper sulfides that are the most commonly employed electrocatalysts for the counter electrode of QDSSCs. Given that the physical properties of copper sulfides are governed by their stoichiometry, the electrocatalytic activity of copper sulfides toward polysulfide reduction may also be dictated by their compositions. Using a new, simple approach to prepare robust copper sulfide films based on chemical bath deposition (CBD), we were able to delicately control the compositions of copper sulfides, which allowed us to perform a systematic investigation to gain new insight into copper sulfide-based electrocatalysts. The electrocatalytic activity is indeed dependent on the compositions of copper sulfides: Cu-deficient films (CuS and $Cu_{1.12}S$) are superior to Cu-rich films ($Cu_{1.75}S$ and $Cu_{1.8}S$) in their electrocatalytic activity. In addition, the stability of the Cu-deficient electrocatalysts is substantially better than that of the Cu-rich counterparts.

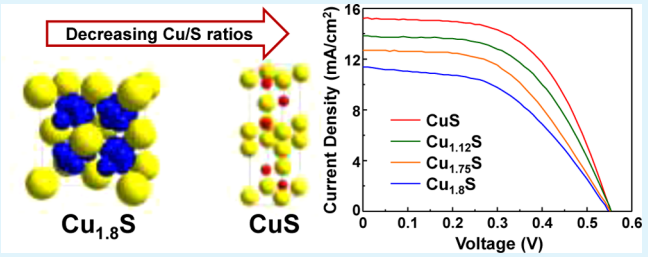

KEYWORDS: *counter electrode, copper sulfides, electrocatalyst, composition, stability*

1. INTRODUCTION

To meet urgent demand for clean energy, extensive research efforts have been made for solar energy conversion systems that can allow for high conversion efficiency. Among them, QDSSCs, a modified version of dye-sensitized solar cells (DSSCs), have long been investigated because of simple fabrication, low cost, and intriguing physical properties of quantum dots (QDs) (e.g., high extinction coefficient and multiple exciton generation) that could boost the stagnant photoconversion efficiency.[1−4] Despite significant strides in the QDSSC research field over a decade, the conversion efficiency of the state-of-the-art QDSSC has just recently attained ∼7%.[5−7] To diagnose bottlenecks and provide a new breakthrough for further development, one needs to carefully re-examine a series of interfacial charge transfer processes occurring during the operation of QDSSC. The interfacial charge transfer processes involve the injection of photogenerated electrons into the conduction band of titanium dioxide (TiO_2) or zinc oxide (ZnO), the scavenging of holes left in QDs by a redox electrolyte (typically the sulfide/polysulfide couple), and regeneration of the redox couple on the counter electrode (CE).[8,9] Inefficient interfacial charge transfer processes often encountered in both photoanodes and CEs, primarily hindered by charge recombination, have been generally considered to be a major limiting factor of QDSSCs.[10−12] With the aid of laser spectroscopy and various electrochemical techniques, a great deal of underlying aspects of interfacial charge transfer and recombination in the photoanode have been revealed.[13−23] However, compared to the interest and achievement in the photoanode, the CE has received little attention except for efforts toward the development of alternative electrocatalysts that can replace platinum (Pt). The key issue in CEs is the poor electrocatalytic activity of CE materials primarily because of the undesirable chemisorption of sulfur species on the electrocatalyst.[24] Pt suffers severely from the surface corrosion, thus substantially deteriorating its ability of interfacial electron transfer for polysulfide reduction. Various metal chalcogenides have been proposed to replace Pt,[25−43] among which cuprous sulfide (Cu_2S) has been commonly employed due to its excellent electrocatalytic activity. Despite the general consensus of using Cu_2S for the fabrication of efficient QDSSCs, the fundamental knowledge of this material is surprisingly lacking. In fact, the use of metal sulfides (e.g., Cu_2S, CoS, and PbS) was first suggested in a report by the

Received: August 14, 2014
Accepted: November 25, 2014
Published: November 25, 2014

Hodes group in 1980.[44] Since then, most of the reports on CE materials have been confined to the nanostructuring of electrocatalysts or the development of new synthesis routes.[45−48] Little is known regarding the intrinsic electrochemical properties of Cu_2S. Even the structural information on Cu_2S has been misled to the QDSSC research community, because our X-ray diffraction (XRD) analysis (Figure S1 in Supporting Information (SI)) of Cu_2S formed by the typical procedure (dipping brass foil or Cu film deposited on F-doped SnO_2 (FTO) glass in a polysulfide solution) revealed not Cu_2S, but $Cu_{1.75}S$. A better understanding of the so-called Cu_2S is therefore urgently required to further advance QDSSCs.

In particular, special attention is given to various compositions available for copper sulfides (Cu_xS) in this work. Along with the stoichiometric end members of Cu_2S (chalcocite) and CuS (covellite), copper sulfides possess a wide range of intermediate phases in between Cu_2S and CuS, which include $Cu_{1.96}S$ (djurleite), $Cu_{1.8}S$ (digenite), $Cu_{1.75}S$ (anilite), and $Cu_{1.12}S$ (yarrowite).[49] The optical, electrical, and thermal properties of copper sulfides is heavily dependent on their compositions, and these intriguing composition-dependent physical properties have been extensively investigated for various applications.[50] We speculated that this rich stoichiometry of copper sulfides may also have a close relationship to their electrocatalytic activity for polysulfide reduction ($S_n^{2-} + 2e^- \rightarrow S_{n-1}^{2-} + S^{2-}$) when utilized as electrocatalysts for QDSSC. To prove our hypothesis, a systematic investigation was performed by delicately controlling the compositions of copper sulfide. Our study revealed that the electrocatalytic activity of Cu_xS is indeed dictated by their compositions, and the stability of Cu_xS is substantially governed by the stoichiometry as well.

2. EXPERIMENTAL SECTION

2.1. Preparation of Cu_xS Films for CEs. Copper sulfides with various compositions were deposited on FTO glass (Pilkington TEC 15, Hartford Glass, Inc.) by a CBD method. Prior to CBD, FTO glass was sequentially cleaned with hydrochloric acid, acetone, ethanol, and deionized water under sonication for 30 min each. For the deposition of Cu_xS films, 0.1 M $CuSO_4$ and 0.1 M $Na_2S_2O_3$ aqueous solution mixed with different volume ratios (CuS = 1:4, $Cu_{1.12}S$ = 1:2.5, $Cu_{1.75}S$ = 1:1.5, and $Cu_{1.8}S$ = 1:1) and the pH of the mixed solutions was adjusted by adding acetic acid to 2 (for CuS and $Cu_{1.12}S$) and 4 (for $Cu_{1.75}S$ and $Cu_{1.8}S$), respectively. FTO glass was then dipped into the solutions held at 70 °C for 3 h, rinsed with deionized water after the reaction, and dried. Finally, the films were annealed at 130 °C for 30 min under air to improve adhesion and decrease the sheet resistance.[51] The weight of copper sulfides deposited on the FTO glass was measured by a microbalance (A&D BM-22, readability to 1 μg). The average mass of the deposited copper sulfides was ∼0.40 mg for all films.

2.2. Fabrication of Solar Cells and Symmetric Dummy Cells. TiO_2-based photoanodes sensitized with CdS/CdSe were prepared via successive ionic layer adsorption and reaction (SILAR) according to our previous work.[30] Polysulfide electrolyte (2 M S, 2 M Na_2S, and 0.1 M NaOH) was prepared by dissolving sulfur in an aqueous Na_2S and NaOH solution. The CdS/CdSe-sensitized photoelectrodes and Cu_xS-based CEs were assembled with a 60-μm Surlyn spacer (Solaronix) into full cells. The polysulfide electrolyte was then injected into the cells via a vacuum backfilling technique. For electrochemical impedance spectroscopy (EIS) and Tafel measurements, symmetric dummy cells were fabricated by assembling two identical CEs face-to-face and filling the polysulfide electrolyte in the same manner.

2.3. Characterization. The identification of Cu_xS was performed by XRD analysis and Raman spectroscopy using an X-ray diffractometer (Rigaku D/Max-2500/PC) and a Renishaw 2000 confocal Raman microscope system, respectively. Diffuse reflectance ultraviolet−visible (UV−vis) absorption spectra of Cu_xS films were measured by a UV−vis spectrophotometer (SCINCO S-3100) equipped with a diffuse reflector (SCINCO). The morphology of Cu_xS films and their compositions were examined by scanning electron microscopy (SEM) using a field-emission scanning electron microscope (FESEM; Hitachi S-4800) equipped with an energy-dispersive X-ray spectroscopy (EDS) detector. X-ray absorption fine structure (XAFS) measurements were performed on 7D beamline of the Pohang Accelerator Laboratory (PLS-II, 3.0 GeV, Korea) to investigate the local structures of copper sulfides. The X-ray absorption spectra for the K-edge of Cu (E_0 = 8980 eV) were acquired in a fluorescence mode at room temperature under an atmosphere of helium. The incident beam was monitored with He-filled IC Spec ionization chamber and fluorescence signal from the samples with PIPS (passivated implanted planar silicon) detector attached to a sample chamber. The spectra of standard CuS and Cu_2S were also measured for comparison. The obtained spectra were analyzed with ATHENA and ARTEMIS in the IFEFIT suite of software programs. FEFF 9 code was used to simulate theoretical extended X-ray absorption fine structure (EXAFS) spectra for nonlinear square fittings of the samples. To examine the oxidation states of copper sulfides, X-ray photoelectron spectroscopy (XPS) measurements were executed using a PHI Versa Probe system with a 100 W Al K Alpha X-ray source. The solar cell performance was evaluated under 1-sun illumination (air mass 1.5G) supplied by a solar simulator (HAL-320, Asahi Spectra). Photocurrent-photovoltage (J−V) curves were recorded using a Keithley 2400 source meter. The active area of the solar cells was 0.20 cm^2 and a black mask was placed over the solar cells to prevent stray light from reaching the cells. EIS, Tafel polarization curve measurements, and cyclic voltammetry (CV) were performed with a potentiostat (CH Instruments, CHI 660D electrochemical workstation). EIS spectra were measured under a frequency range from 0.1 Hz to 100 kHz and a perturbation amplitude of 10 mV. Tafel polarization curves were obtained at a scan rate of 50 $mV{\cdot}s^{-1}$.

3. RESULTS AND DISCUSSION

A common procedure for the preparation of the widely used Cu_2S CE is based on an in situ reaction between Cu and polysulfide. While this approach is simple and reproducible, thin Cu_2S film formed on brass foil or FTO glass often suffers from mechanical instability (Figure S2 in SI). Alternative methods to tackle this problem include electrodeposition, SILAR, and the doctor-blading (or spin coating) of Cu_2S/carbon composites; however, the delicate tuning of the ratios of Cu/S is hardly achievable by these methods.[30,47,48] We therefore tried a new approach based on CBD, which offers composition-tunability and produces robust films with high reproducibility. Cu_xS films with various compositions were deposited on FTO glass using copper thiosulfate baths, where the thiosulfate acts as a sulfide ion source and a complexing agent to prevent the instantaneous precipitation of copper ions with sulfide ions.[51] A reaction mechanism for the Cu_xS deposition is proposed as follows: (1) electron release from $S_2O_3^{2-}$, (2) dissociation of $S_2O_3^{2-}$ with the aid of protons, (3) the formation of S^{2-}, and (4) the reaction of Cu^{2+} and S^{2-}.[52]

$$2S_2O_3^{2-} \rightarrow S_4O_6^{2-} + 2e^- \quad (1)$$

$$S_2O_3^{2-} + H^+ \rightarrow HSO_3^- + S \quad (2)$$

$$S + 2e^- \rightarrow S^{2-} \quad (3)$$

$$xCu^{2+} + S^{2-} \rightarrow Cu_xS \quad (4)$$

Cu_xS films were preferentially deposited only on the FTO-coated side of glass, which was ascribed to the rough surface of the FTO-coated side that eases nucleation. According to the proposed mechanism, the pH of copper thiosulfate baths plays a critical role in the controlled release of S^{2-} along with the concentration of thiosulfate. This controlled release of S^{2-} by the simple variation in concentration and pH allowed the preparation of robust Cu_xS films with various compositions that would have barely been achievable by other common methods.

Figure 1 displays the UV−vis absorption spectra and photographs of four kinds of Cu_xS films (CuS, $Cu_{1.12}S$, $Cu_{1.75}S$, and $Cu_{1.8}S$) deposited by CBD. Depending on their compositions, each film exhibited unique colors that were reflected in the UV−vis absorption spectra. Cu-deficient films (CuS and $Cu_{1.12}S$) show stronger absorption in the near-infrared region than Cu-rich films ($Cu_{1.75}S$ and $Cu_{1.8}S$), which originates from free-carrier intraband absorption.[50,53] The deposition of Cu_2S film by manipulating the concentration of thiosulfate and pH was unsuccessful in multiple trials, which was attributed to the instability of Cu_2S under ambient condition. The partial oxidation of Cu^+ by oxygen leads to the formation of metastable $Cu_{1.8}S$ (or $Cu_{1.75}S$) rather than Cu_2S.[54−56] The $Cu_{1.75}S$ formation rather than Cu_2S during the common Cu_2S preparation method may be relevant to this inherent instability of Cu_2S.

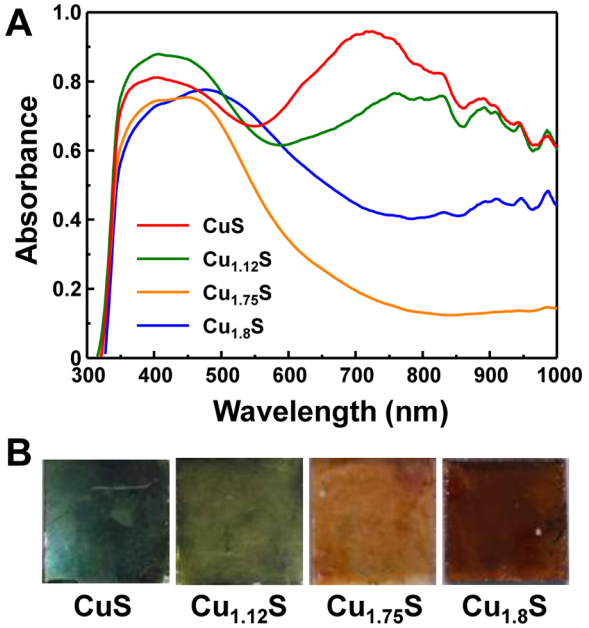

Figure 1. (A) UV−vis absorption spectra and (B) photographs of copper sulfides: CuS, $Cu_{1.12}S$, $Cu_{1.75}S$, and $Cu_{1.8}S$.

The crystal structure of the four films was examined by XRD analysis (Figure 2A). While the Cu_xS films showed distinctly different colors, the identification of crystallographic phases of Cu_xS with similar compositions was a bit difficult because of the resemblance in diffraction patterns. However, there are negligible deviations in cell parameters when comparing our calculated lattice parameters with those of standard samples (Table S1 in SI), confirming the successful formation of different crystallographic phases by CBD. The diffraction pattern of CuS film matched hexagonal covellite (JCPDS 79-2321, space group $P6_3/mmc$, $a = b = 3.788$ Å, $c = 16.333$ Å) and $Cu_{1.12}S$ film was assigned to standard yarrowite (JCPDS 36-0379, space group $P\bar{3}m1$, a=b=3.8 Å, c=67.269 Å). The diffraction patterns of $Cu_{1.75}S$ and $Cu_{1.8}S$ were designated to orthorhombic anilite (JCPDS 33−0489, space group *Pnma*, $a = 7.901$ Å, $b = 7.822$ Å, $c = 11.078$ Å) and digenite (JCPDS 47-1748, space group $R\bar{3}m$, $a = b = 3.93$ Å, $c = 48.14$ Å), respectively. The subtle difference observed in the XRD patterns was also reflected in the Raman spectra (Figure 2B), where there was a slight shift of the intense peak at ~471 cm^{-1} (resulting from a S−S stretching mode) to larger wavenumbers with a decrease in the ratios of Cu/S. This trend was consistent with a recent report on the Raman spectroscopy of the Cu−S system with different compositions.[49]

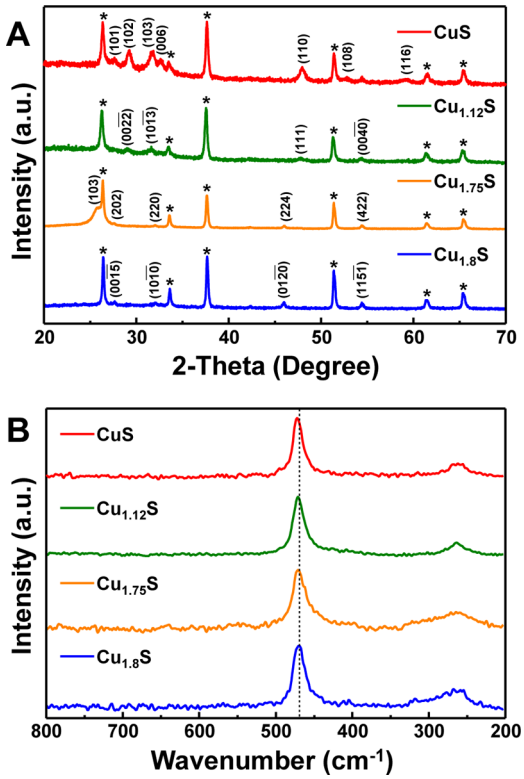

Figure 2. (A) XRD patterns (peaks from the FTO substrate are marked with asterisks) and (B) Raman spectra of copper sulfides: CuS, $Cu_{1.12}S$, $Cu_{1.75}S$, and $Cu_{1.8}S$.

The morphology of the four Cu_xS films was examined by SEM analysis (Figure 3). The SEM images (also see low magnification images in Figure S3 in SI) show that all films were fully covered with Cu_xS particles. The SEM cross-section images (Figure S4 in SI) revealed that all films became thicker gradually as the CBD reaction proceeded, and the film thickness was as thick as ~2 μm after 3 h reaction. This observation indicates that the thickness of Cu_xS films can be controlled simply by changing reaction times. Compared to the Cu-deficient films (CuS and $Cu_{1.12}S$), the Cu-rich films ($Cu_{1.75}S$ and $Cu_{1.8}S$) were mostly made of slightly larger grains. The composition of each film was obtained by EDS analysis (Table S2 in SI), where all the Cu/S ratios were consistent with the ratios affirmed by other analyses within the margin of error.

X-ray absorption spectroscopy (XAS) was performed to examine the local geometric structure and electronic structure of Cu_xS films. The Cu K-edge X-ray absorption near edge structure (XANES) spectra of the Cu-deficient films (CuS and $Cu_{1.12}S$) are shown in Figure 4A. Both spectra resembled the XANES spectrum of standard CuS, verifying the composition

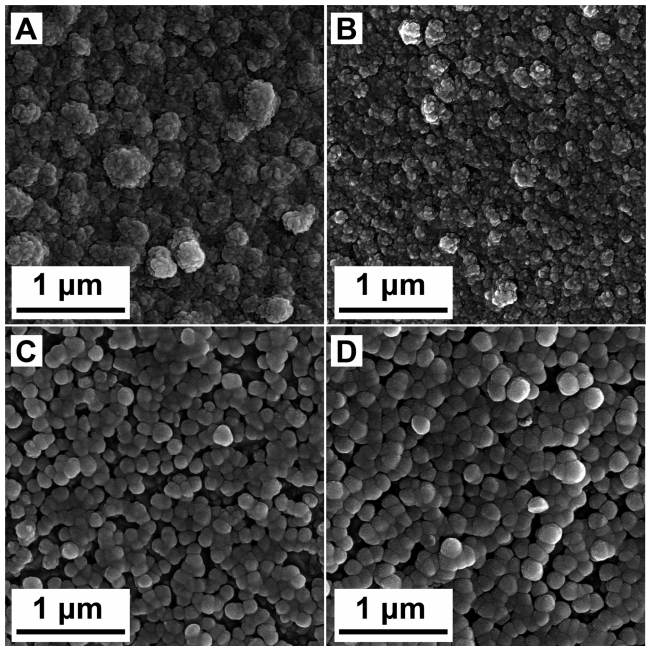

Figure 3. SEM images of copper sulfides: (A) CuS, (B) $Cu_{1.12}S$, (C) $Cu_{1.75}S$, and (D) $Cu_{1.8}S$.

analysis results acquired by various characterization techniques. Notably, a pre-edge was observed at ~8979 eV just before the intense rising edge arose, which resulted from the electric-dipole forbidden, quadruple-allowed 1s-3d transition. In general, the oxidation state of Cu in CuS is designated as Cu(I) with the electronic configuration of $3d^{10}$.[57] Since this quadruple transition can appear only in the presence of the Cu(II) state with the electronic configuration of $3d^9$,[58] this observation suggested the presence of Cu(II) character in the CuS and $Cu_{1.12}S$ films. The XANES spectra of $Cu_{1.75}S$ and $Cu_{1.8}S$ (Figure 4B) were similar to that of standard Cu_2S, thus confirming their determined compositions. Figure 4C displays the Fourier-transformed EXAFS spectra of Cu_xS films. The fitting parameters are summarized in Table S3 in SI. The main peak (denoted as (a)) at 0.8−2.3 Å in the spectra accounts for Cu−S scattering. The Cu-deficient films (CuS and $Cu_{1.12}S$) showed higher peak intensities than the Cu-rich films ($Cu_{1.75}S$ and $Cu_{1.8}S$), which can be correlated to smaller Debye−Waller factors, which is an indication of disorder.[58] As the XAS measurements were performed at the same temperature, this factor can be directly correlated to the degree of structural disorder. Another noticeable difference between the Cu-deficient films and Cu-rich films is the presence of a small peak at 2.6−3.5 Å (denoted as (b)) that appeared only for CuS and $Cu_{1.12}S$ films, which is also related to structural disorder. According to the fitting parameters, CuS and $Cu_{1.12}S$ exhibited smaller Debye−Waller factors than $Cu_{1.75}S$ and $Cu_{1.8}S$, which is in accordance with the disparity in the EXAFS spectra. This implies that CuS and $Cu_{1.12}S$ have more ordered structures than $Cu_{1.75}S$ and $Cu_{1.8}S$. The disorder in the Cu-rich films is presumably related to the relatively high mobility of copper ions in sulfide.[59]

The characterization through various spectroscopic and micrographic analyses verified the subtle variation in the compositions of each Cu_xS film, and proved the usefulness of the CBD method for its composition-tunability. While these analyses provided informative insight into bulk compositions,

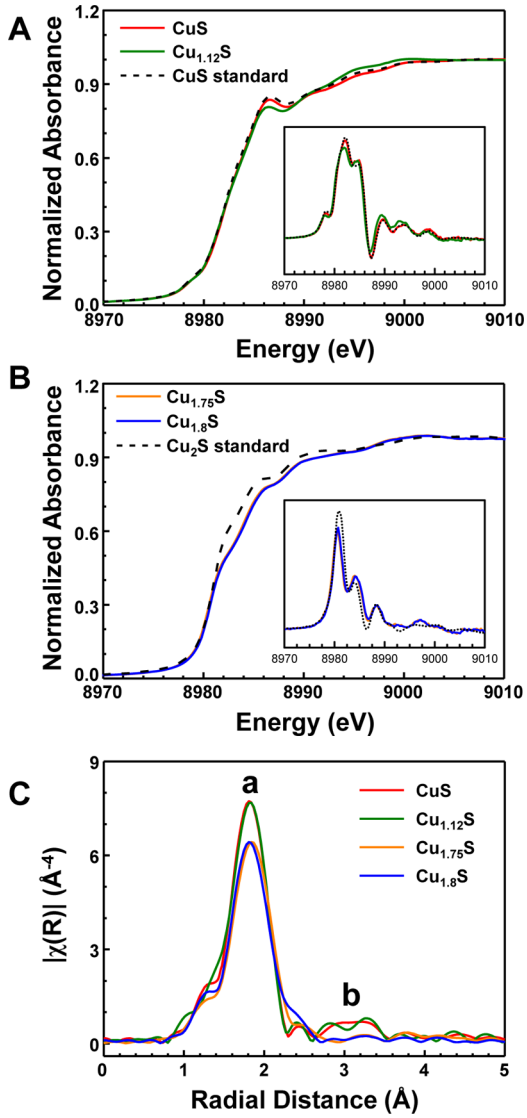

Figure 4. Cu K-edge XANES spectra of copper sulfides: (A) CuS and $Cu_{1.12}S$ and (B) $Cu_{1.75}S$ and $Cu_{1.8}S$ (inset: respective derivative spectra); CuS and Cu_2S standards are also displayed in (A) and (B), respectively; (C) k^3-weighted Fourier transforms of Cu K-edge EXAFS for copper sulfides.

they cannot provide any information on the surface characteristics of Cu_xS films. Given that electrocatalytic reactions occur on the surface of catalyst films and thus the electrocatalytic activity is intimately related to the surface state of electrocatalysts,[30] the investigation of the surface properties of Cu_xS films is essential in understanding their electrocatalytic activity. As a result, XPS analysis was performed to explore the surface state of each film. Figure 5A displays the Cu 2p spectra of four Cu_xS films, where the two strong peaks at ~932 and ~952 eV were assigned to the binding energy of Cu $2p_{3/2}$ and Cu $2p_{1/2}$, respectively. There were small shakeup satellite peaks at ~944 eV in all of the spectra, which is an evidence of divalent Cu species. As the amount of Cu increased, a small peak gradually developed at ~935 eV, which was attributed to the oxidized species of Cu such as CuO and $CuSO_4$. This surface oxidation in the Cu-rich films was also observed in the S 2p spectra (Figure 5B). As opposed to the CuS and $Cu_{1.12}S$ films, $Cu_{1.75}S$ and $Cu_{1.8}S$ films exhibited a distinctive peak at 168.6 eV because of the presence of oxidized S species such as SO_4^{2-}.[60]

dx.doi.org/10.1021/am505473d | ACS Appl. Mater. Interfaces 2014, 6, 22078−22087

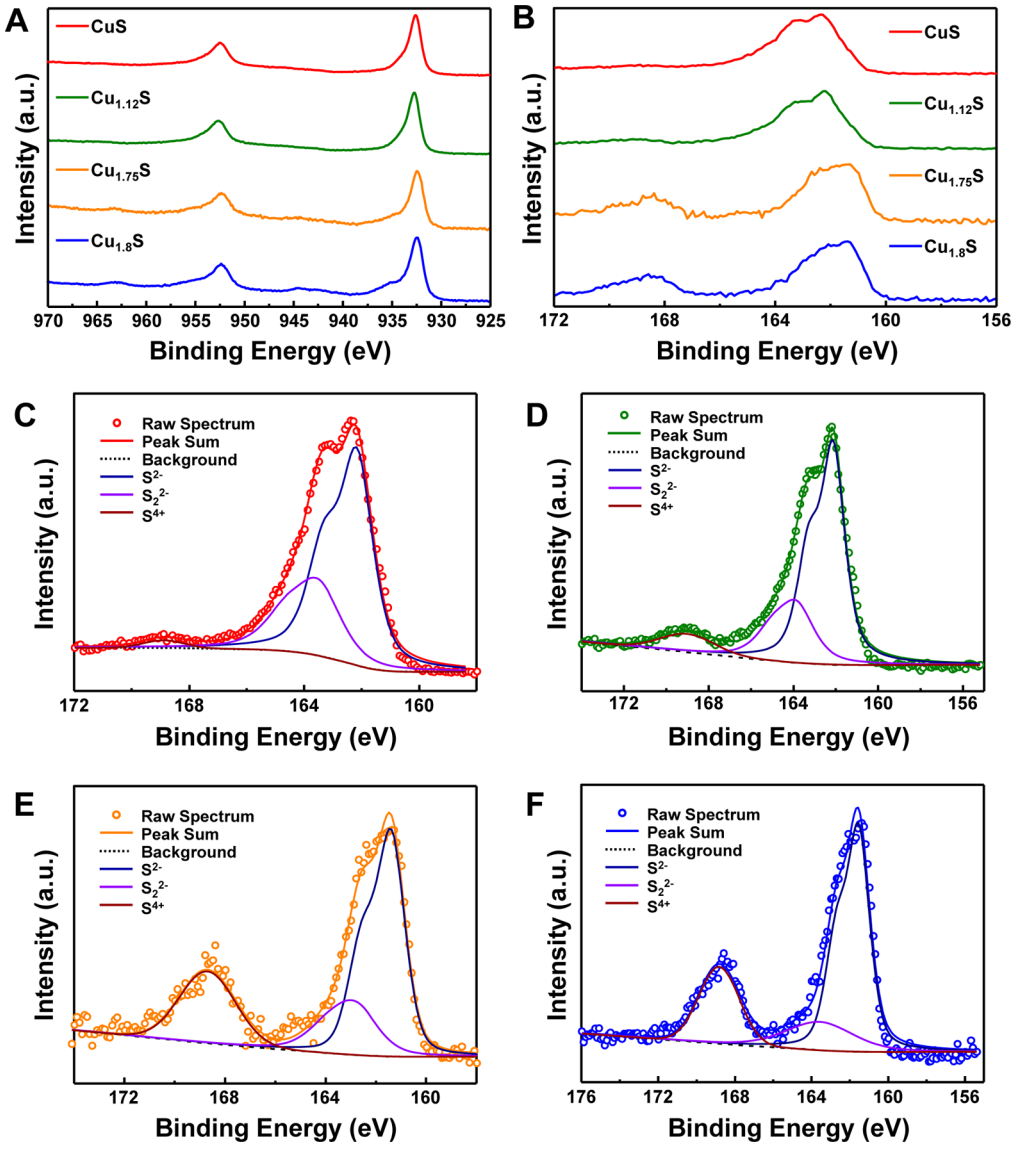

Figure 5. XPS spectra of copper sulfides: (A) Cu 2p and (B) S 2p regions. Fitted S 2p spectra of (C) CuS, (D) $Cu_{1.12}S$, (E) $Cu_{1.75}S$, and (F) $Cu_{1.8}S$.

To gain more insight into the surface oxidation, the S 2p band of each film was deconvoluted into three peaks: a main doublet at 162.2 eV designated for sulfide (S^{2-}), another doublet at 163.7 eV for disulfide (S_2^{2-}), and a third peak at 168.8 eV for the oxidized S species (Figures 5C–F). The ratios of sulfide to disulfide became progressively smaller with the increase in the Cu/S ratios of the Cu_xS films, which is consistent with a recent report.[61] The prevalent disulfide component in the Cu-deficient films compared to the Cu-rich films is credited to the presence of S–Cu and S–S bonds (the crystal structure of CuS is composed of a layer of triangular CuS_3 units sandwiched between two layers made of CuS_4 tetrahedra. Each triple layer is then interlinked to each other with disulfide bonds).[58,61] The most important feature to note in the S 2p spectra is the enhanced intensity of the third peak resulting from the surface oxidation as the Cu/S ratios are greater. This suggests that the Cu_xS films become more vulnerable to surface oxidation as they were progressively richer in Cu.

The electrocatalytic activity of Cu_xS films toward polysulfide reduction was investigated by Tafel polarization and EIS measurements using symmetric dummy cells. Figure 6A shows the Tafel polarization curves of each Cu_xS film. The Tafel polarization measurement provides valuable information on charge transfer kinetics, as the exchange current (i_0) estimated from the extrapolated intercepts of the anodic and cathodic branches of the Tafel polarization curves is related to the charge-transfer resistance according to the following equation:

$$i_0 = \frac{RT}{nFR_{ct}} \tag{5}$$

where R is the gas constant, T is the absolute temperature, n is the number of electrons involved in the polysulfide reduction, F is the Faraday constant, and R_{ct} is the charge-transfer resistance. It is clearly evident from Figure 6A that the i_0 value of CuS is the greatest among the four Cu_xS films and the i_0 values gradually decreased with the increased Cu/S ratios. This observation implies that the electrocatalytic activity for the polysulfide reduction does depend on the stoichiometry of copper sulfides. Given the order of i_0 values, CuS film is the most electrocatalytically active toward the polysulfide reduction. The i_0 trend observed in the Tafel polarization curves was affirmed by the EIS measurement. The Nyquist plots obtained

dx.doi.org/10.1021/am505473d | ACS Appl. Mater. Interfaces 2014, 6, 22078–22087

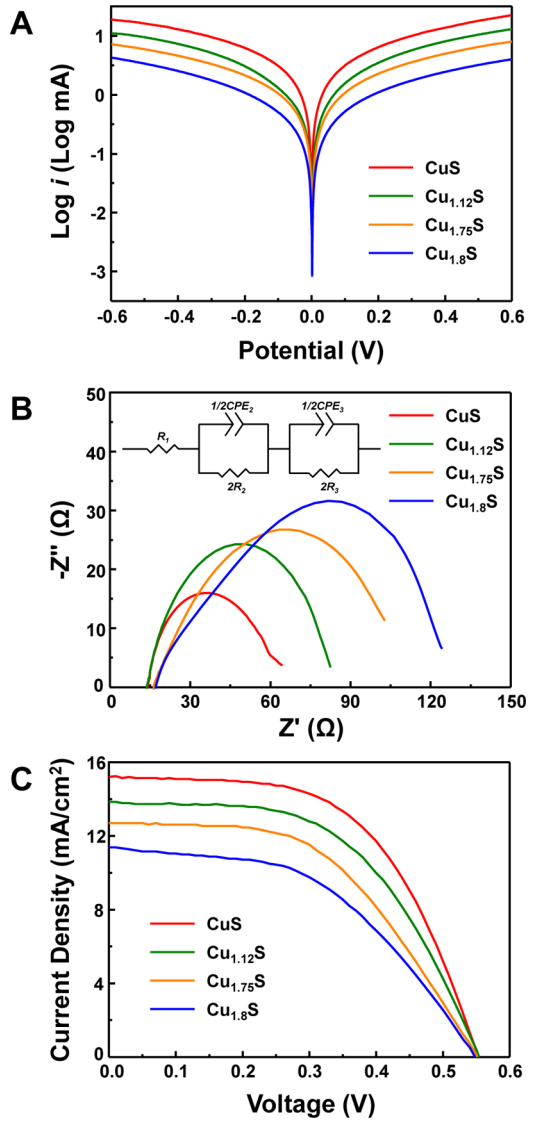

Figure 6. (A) Tafel polarization curves, (B) EIS spectra of Cu_xS (inset shows an equivalent circuit employed to fit the EIS spectra; R_1 = ohmic serial resistance, R_2 = charge-transfer resistance of solid/solid interface (one electrode), R_3 = charge-transfer resistance of electrolyte/CE interface (one electrode), CPE_2 = constant phase angle element of solid/solid interface (one electrode), and CPE_3 = constant phase angle element of electrolyte/CE interface (one electrode)), and (C) $J-V$ curves of QDSSCs with various Cu_xS CEs under 1 SUN (Air Mass 1.5G) illumination.

from the EIS measurement are shown in Figure 6B, and the charge transfer resistances extracted from the equivalent circuit are summarized in Table 1 (the sheet resistances, the resistances associated with the solid−solid interface, and the charge transfer resistances associated with the polysulfide reduction were represented by R_1, R_2, and R_3, respectively).[27,62,63] All the resistances of the Cu_xS films were in the order of CuS, $Cu_{1.12}S$, $Cu_{1.75}S$, and $Cu_{1.8}S$. R_1 reflects the electrical conductivity of Cu_xS films. In general, the electrical conductivity of copper sulfides is governed by the p-type conduction mechanism, in which free holes created by Cu vacancies act as major charge carriers.[51] Since the Cu vacancy increases as x decreases in Cu_xS, the Cu-deficient films possess more metallic character. The trend in R_1 is therefore attributed to this composition-dependent electrical conductivity, which is in accordance with previous works.[51,64] Larger R_2 values in the Cu-rich films may be ascribed to poor connections between Cu_xS particles compared to the Cu-deficient films as evidenced by the SEM images, which impede electron transport through the nanoparticle network as noted previously.[27] The tendency of R_3 values was consistent with the trend observed in the Tafel polarization curves. The validity of R_3 values obtained by EIS was also cross-checked by calculating the i_0 values according to eq 5, which closely match the i_0 values of each Cu_xS film obtained from the Tafel curve measurements (0.327, 0.185, 0.162, and 0.154 mA, respectively). Along with the charge transfer resistances, the morphological difference between Cu-rich and Cu-deficient films may also contribute to the electrocatalytic activity. High magnification SEM images (SI Figure S5) showed that irregular-shaped particles aggregated into a compact layer in the case of Cu-deficient films, whereas spherical agglomerates were interlinked into a porous network in the case of Cu-rich films. This morphological difference was reflected in the EIS parameters. In EIS analysis, interfacial capacitance is described as $Z_{CPE} = A(jw)^{-\alpha}$ $(0 \le \alpha \le 1)$, where w is the angular frequency and A and α are frequency-independent parameters. Constant phase element (CPE_3) is closely associated with the roughness of electrodes, and α parameters are related to the porosity of electrodes.[62,65] CPE_3 values obtained from the Cu-rich films were larger than those from the Cu-deficient films, and α values from the Cu-rich films were smaller than those from the Cu-deficient films (Table S4 in SI). This implies that a greater number of effective electrocatalytic sites that are accessible by the polysulfide electrolyte are available for the Cu-rich films compared to the Cu-deficient films. Given the trend in electrocatalytic activity of Cu_xS films and smaller differences in CPE_3 and α values, however, the influence of the morphological difference on the electrocatalytic activity seems to be negligible as compared to that of the charge transfer resistances.

The series resistance (R_s) of CE in QDSSCs can be defined as the sum of R_1, R_2, and R_3,[40,46] which can significantly affect the performance of solar cells. When the Cu_xS films were employed as CEs for QDSSCs, the influence of R_s (mostly contributed to by R_3 that is related to the electrocatalytic activity of Cu_xS films) was clearly reflected in the current−voltage ($J-V$) curves of QDSSCs (Figure 6C). The solar cell parameters, short-circuit current (J_{sc}), open-circuit voltage (V_{oc}), fill factor (FF), and power conversion efficiency (η), are summarized in Table 1. Note that multiple cells were fabricated and measured to ensure the reproducibility of our results (see multiple measurement results in Table S5 in SI). Consistent with the results of Tafel polarization and EIS measurements, the QDSSC equipped with the CuS film as the CE showed the best performance, and the enhanced η with the Cu-deficient films was accounted for by the improved J_{sc} and FF that were substantially influenced by R_s. This result clearly

Table 1. Solar Cell Parameters of QDSSCs with Various Cu_xS CEs and Resistances of Cu_xS Electrodes Obtained from EIS Analysis

counter electrode	J_{sc} (mA/cm^2)	V_{oc} (V)	FF	η (%)	R_1 (Ω)	$2R_2$ (Ω)	$2R_3$ (Ω)
CuS	15.2	0.554	0.56	4.75	14.0	13.8	39.3
$Cu_{1.12}S$	13.8	0.554	0.54	4.13	13.8	16.0	69.3
$Cu_{1.75}S$	12.7	0.552	0.51	3.56	16.3	17.8	79.3
$Cu_{1.8}S$	11.4	0.547	0.48	3.01	16.9	26.3	83.4

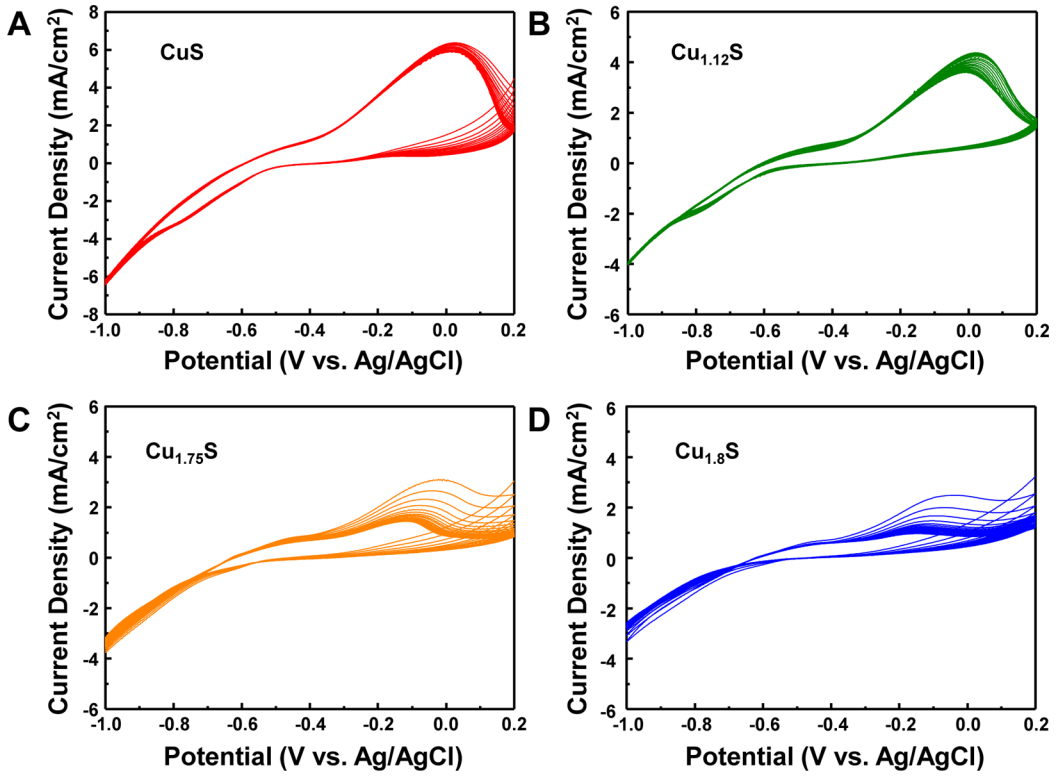

Figure 7. Cyclic voltammograms of (A) CuS, (B) $Cu_{1.12}S$, (C) $Cu_{1.75}S$, and (D) $Cu_{1.8}S$ electrodes taken under a three-electrode system with the Ag/AgCl reference electrode, the Pt counter electrode, and polysulfide electrolyte (0.1 M S, 0.1 M Na_2S, 5 mM NaOH solution) at a scan rate of 50 mV/s.

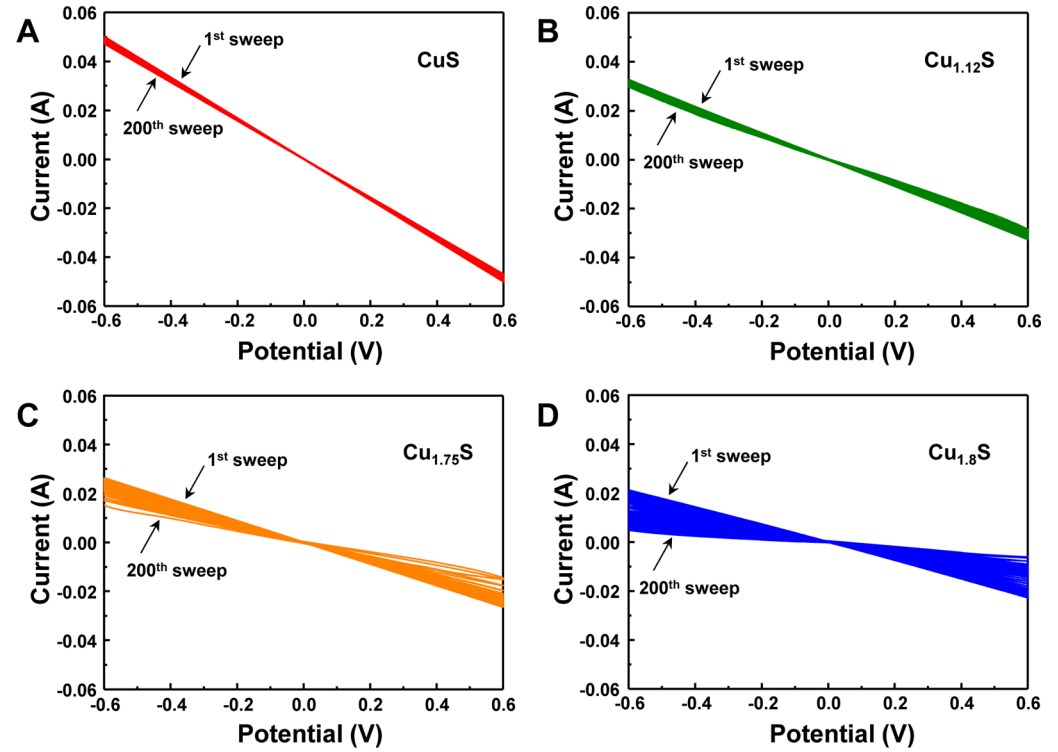

Figure 8. Stability test results of (A) CuS, (B) $Cu_{1.12}S$, (C) $Cu_{1.75}S$, and (D) $Cu_{1.8}S$ performed by continuous potential sweeping of each symmetric dummy cell at a scan rate of 100 mV/s.

demonstrated the composition effect of Cu_xS on the performance of QDSSC. To eliminate a possibility of the contribution from dark current (i.e., small current flowing through a solar cell in the absence of light illumination) to the enhanced J_{sc}, we examined dark currents of the QDSSCs (Figure S6 in SI). There were negligible dark currents observed with all QDSSCs,

dx.doi.org/10.1021/am505473d | ACS Appl. Mater. Interfaces 2014, 6, 22078−22087

confirming that the difference in solar cell performance stems mainly from the Cu_xS CEs.

Cyclic voltammetry (CV) was performed under a three-electrode system using a diluted polysulfide (0.1 M S, 0.1 M Na_2S, and 5 mM NaOH) electrolyte to elucidate the redox processes on the Cu_xS films. Figure 7 shows the cyclic voltammograms of four Cu_xS electrodes. As noted by Kamat and co-workers, the surface concentrations of the reduced and oxidized polysulfide species were consumed to the extent that Nerstian shifts were observed in the equilibrium potentials with all the Cu_xS electrodes.[48] The magnitudes of the current density for the polysulfide reduction were in the order of CuS, $Cu_{1.12}S$, $Cu_{1.75}S$, and $Cu_{1.8}S$, which is in good agreement with other electrochemical measurement results. Interestingly, a gradual decrease in the current density was observed as the potential cycling proceeded, and this degradation was much more pronounced in the Cu-rich electrodes. This observation led us to investigate the stability of Cu_xS electrodes, because the long-term stability is a vital requirement of CE along with high electrocatalytic activity. Symmetric dummy cells made of identical Cu_xS electrodes and the polysulfide electrolyte with the same concentrations as the electrolyte used for QDSSCs were used to evaluate the stability. Figure 8 shows current−voltage responses of Cu_xS electrodes during continuous potential sweeping. Unlike the Cu-deficient electrodes (Figure 8A and 8B), the Cu-rich electrodes exhibited a noticeable decay after 200 potential sweeps (Figure 8C and 8D). This observation revealed that the stability of Cu_xS electrodes is also relevant to their stoichiometry. The instability of the Cu-rich electrodes may be associated with the presence of oxidized Cu and S species on their surface. According to the XPS analysis, the oxidized species on the surface of Cu_xS films were presumably copper(II) sulfate ($CuSO_4$), which can be dissolved into the polysulfide electrolyte ($CuSO_4$ can exothermically dissolve in water to produce the $Cu(H_2O)_6^{2+}$ complex). Since the Cu-rich electrodes are more easily oxidized than the Cu-deficient electrodes, the loss of the Cu_xS particles via the dissolution in the form of $CuSO_4$ is likely to proceed significantly faster in the Cu-rich electrodes. This argument was partly supported by the photographs of Cu_xS electrodes taken after the CV experiment (Figure S7 in SI). While there was no noticeable loss on the CuS electrode, the $Cu_{1.8}S$ electrode suffered from severe loss after continuous potential sweeps. Such instability of metal chalcogenides due to the presence of surface oxides was also observed in our recent work.[30] Further investigation is currently underway to elucidate the instability of the Cu-rich electrodes.

4. CONCLUSIONS

This work presents a new synthesis approach to prepare Cu_xS films on FTO glass that can be exploited for the CE in QDSSCs. Unlike other common methods, the CBD method produced robust films and allowed delicate tuning of the composition of Cu_xS. This composition-tunability allowed for the systematic investigation of the composition-dependent electrocatalytic activity of Cu_xS with various stoichiometries. The in-depth characterization combined with electrochemical analyses revealed for the first time that the subtle difference in the Cu/S ratios played a critical role in dictating the electrocatalytic activity toward polysulfide reduction. The CuS film was superior to other Cu_xS films, and the electrocatalytic activity of Cu_xS films decreased as the amount of Cu in the Cu_xS films became progressively richer. Our work also revealed that the stability of Cu_xS films was related to their stoichiometry. The Cu-deficient electrodes (CuS and $Cu_{1.12}S$) were significantly more stable than the Cu-rich counterparts ($Cu_{1.75}S$ and $Cu_{1.8}S$), which was attributed to their greater resistance against surface oxidation. These new insights into Cu_xS-based electrocatalysts may pave the way for further development of QDSSCs.

■ ASSOCIATED CONTENT

Supporting Information

XRD pattern of copper sulfide fabricated by dipping Cu film on FTO into a Na_2S solution; photographs of Cu_2S electrodes fabricated by conventional methods before and after solar cell operation; lattice parameters calculated from XRD patterns; atomic ratios of copper sulfides determined by SEM−EDS quantitative analysis; additional SEM images of copper sulfides; SEM cross-sectional images of each Cu_xS film taken at different CBD reaction times; structural parameters calculated from Cu K-edge EXAFS fits of copper sulfides; solar cell parameters of QDSSCs (from multiple measurements); high magnification SEM images of copper sulfides; CPE_3 and α_3 values of Cu_xS electrodes obtained from EIS analysis; photographs of Cu_xS electrodes after cyclic voltammetry experiment. This material is available free of charge via the Internet at http://pubs.acs.org.

■ AUTHOR INFORMATION

Corresponding Author

*E-mail: jbang@hanyang.ac.kr.

Notes

The authors declare no competing financial interest.

■ ACKNOWLEDGMENTS

This research was supported by the grants from the Basic Science Research Program (NRF-2013R1A1A1008762) through the National Research Foundation of Korea (NRF) funded by the Ministry of Science, ICT and Future Planning. XAS Experiments at PLS-II 7D XAFS beamline were supported in part by MEST and POSTECH.

■ REFERENCES

(1) Kamat, P. V. Quantum Dot Solar Cells. The Next Big Thing in Photovoltaics. *J. Phys. Chem. Lett.* **2013**, *4*, 908−918.

(2) Hodes, G. Comparison of Dye- and Semiconductor-Sensitized Porous Nanocrystalline Liquid Junction Solar Cells. *J. Phys. Chem. C* **2008**, *112*, 17778−17787.

(3) Yang, Z.; Chen, C.-Y.; Roy, P.; Chang, H.-T. Quantum Dot-Sensitized Solar Cells Incorporating Nanomaterials. *Chem. Commun.* **2011**, *47*, 9561−9571.

(4) Hetsch, F.; Xu, X.; Wang, H.; Kershaw, S. V.; Rogach, A. L. Semiconductor Nanocrystal Quantum Dots as Solar Cell Components and Photosensitizers: Material, Charge Transfer, and Separation Aspects of Some Device Topologies. *J. Phys. Chem. Lett.* **2011**, *2*, 1879−1887.

(5) Pan, Z.; Mora-Seró, I.; Shen, Q.; Zhang, H.; Li, Y.; Zhao, K.; Wang, J.; Zhong, X.; Bisquert, J. High-Efficiency "Green" Quantum Dot Solar Cells. *J. Am. Chem. Soc.* **2014**, *136*, 9203−9210.

(6) Pan, Z.; Zhao, K.; Wang, J.; Zhang, H.; Feng, Y.; Zhong, X. Near Infrared Absorption of $CdSe_xTe_{1-x}$ Alloyed Quantum Dot Sensitized Solar Cells with More than 6% Efficiency and High Stability. *ACS Nano* **2013**, *7*, 5215−5222.

(7) Wang, J.; Mora-Seró, I.; Pan, Z.; Zhao, K.; Zhang, H.; Feng, Y.; Yang, G.; Zhong, X.; Bisquert, J. Core/Shell Colloidal Quantum Dot Exciplex States for the Development of Highly Efficient Quantum-Dot-Sensitized Solar Cells. *J. Am. Chem. Soc.* **2013**, *135*, 15913−15922.

(8) Kamat, P. V. Boosting the Efficiency of Quantum Dot Sensitized Solar Cells through Modulation of Interfacial Charge Transfer. *Acc. Chem. Res.* **2012**, *45*, 1906−1915.
(9) Hod, I.; Zaban, A. Materials and Interfaces in Quantum Dot Sensitized Solar Cells: Challenges, Advances and Prospects. *Langmuir* **2013**, *30*, 7264−7273.
(10) Mora-Seró, I.; Giménez, S.; Fabregat-Santiago, F.; Gómez, R.; Shen, Q.; Toyoda, T.; Bisquert, J. Recombination in Quantum Dot Sensitized Solar Cells. *Acc. Chem. Res.* **2009**, *42*, 1848−1857.
(11) Bang, J. H.; Kamat, P. V. CdSe Quantum Dot−Fullerene Hybrid Nanocomposite for Solar Energy Conversion: Electron Transfer and Photoelectrochemistry. *ACS Nano* **2011**, *5*, 9421−9427.
(12) González-Pedro, V.; Xu, X.; Mora-Seró, I.; Bisquert, J. Modeling High-Efficiency Quantum Dot Sensitized Solar Cells. *ACS Nano* **2010**, *4*, 5783−5790.
(13) Robel, I.; Subramanian, V.; Kuno, M.; Kamat, P. V. Quantum Dot Solar Cells. Harvesting Light Energy with CdSe Nanocrystals Molecularly Linked to Mesoscopic TiO_2 Films. *J. Am. Chem. Soc.* **2006**, *128*, 2385−2393.
(14) Bang, J. H.; Kamat, P. V. Quantum Dot Sensitized Solar Cells. A Tale of Two Semiconductor Nanocrystals: CdSe and CdTe. *ACS Nano* **2009**, *3*, 1467−1476.
(15) Barea, E. M.; Shalom, M.; Giménez, S.; Hod, I.; Mora-Sero, I. n.; Zaban, A.; Bisquert, J. Design of Injection and Recombination in Quantum Dot Sensitized Solar Cells. *J. Am. Chem. Soc.* **2010**, *132*, 6834−6839.
(16) Yan, K.; Zhang, L.; Qiu, J.; Qiu, Y.; Zhu, Z.; Wang, J.; Yang, S. A Quasi-Quantum Well Sensitized Solar Cell with Accelerated Charge Separation and Collection. *J. Am. Chem. Soc.* **2013**, *135*, 9531−9539.
(17) Yu, X.-Y.; Liao, J.-Y.; Qiu, K.-Q.; Kuang, D.-B.; Su, C.-Y. Dynamic Study of Highly Efficient CdS/CdSe Quantum Dot-Sensitized Solar Cells Fabricated by Electrodeposition. *ACS Nano* **2011**, *5*, 9494−9500.
(18) Shalom, M.; Buhbut, S.; Tirosh, S.; Zaban, A. Design Rules for High-Efficiency Quantum-Dot-Sensitized Solar Cells: A Multilayer Approach. *J. Phys. Chem. Lett.* **2012**, *3*, 2436−2441.
(19) McDaniel, H.; Fuke, N.; Makarov, N. S.; Pietryga, J. M.; Klimov, V. I. An Integrated Approach to Realizing High-Performance Liquid-Junction Quantum Dot Sensitized Solar Cells. *Nat. Commun.* **2013**, *4*, 2887.
(20) Bang, J. H.; Kamat, P. V. Solar Cells by Design: Photoelectrochemistry of TiO_2 Nanorod Arrays Decorated with CdSe. *Adv. Funct. Mater.* **2010**, *20*, 1970−1976.
(21) Tvrdy, K.; Frantsuzov, P. A.; Kamat, P. V. Photoinduced Electron Transfer from Semiconductor Quantum Dots to Metal Oxide Nanoparticles. *Proc. Nat. Acad. Sci. U.S.A.* **2011**, *108*, 29−34.
(22) Bang, J. H. Influence of Nanoporous Oxide Substrate on the Performance of Photoelectrode in Semiconductor-Sensitized Solar Cells. *Bull. Korean Chem. Soc.* **2012**, *33*, 4063−4068.
(23) Meng, K.; Surolia, P. K.; Thampi, K. R. $BaTiO_3$ Photoelectrodes for CdS Quantum Dot Sensitized Solar Cells. *J. Mater. Chem. A* **2014**, *2*, 10231−10238.
(24) Lee, Y.-L.; Lo, Y.-S. Highly Efficient Quantum-Dot-Sensitized Solar Cell Based on Co-Sensitization of CdS/CdSe. *Adv. Funct. Mater.* **2009**, *19*, 604−609.
(25) Yang, Z.; Chen, C.-Y.; Liu, C.-W.; Chang, H.-T. Electrocatalytic Sulfur Electrodes for CdS/CdSe Quantum Dot-Sensitized Solar Cells. *Chem. Commun.* **2010**, *46*, 5485−5487.
(26) Cao, Y.; Xiao, Y.; Jung, J.-Y.; Um, H.-D.; Jee, S.-W.; Choi, H. M.; Bang, J. H.; Lee, J.-H. Highly Electrocatalytic $Cu_2ZnSn(S_{1-x}Se_x)_4$ Counter Electrodes for Quantum-Dot-Sensitized Solar Cells. *ACS Appl. Mater. Interfaces* **2013**, *5*, 479−484.
(27) Yang, Y.; Zhu, L.; Sun, H.; Huang, X.; Luo, Y.; Li, D.; Meng, Q. Composite Counter Electrode Based on Nanoparticulate PbS and Carbon Black: Towards Quantum Dot-Sensitized Solar Cells with Both High Efficiency and Stability. *ACS Appl. Mater. Interfaces* **2012**, *4*, 6162−6168.
(28) Zhang, X.; Huang, X.; Yang, Y.; Wang, S.; Gong, Y.; Luo, Y.; Li, D.; Meng, Q. Investigation on New $CuInS_2$/Carbon Composite Counter Electrodes for CdS/CdSe Cosensitized Solar Cells. *ACS Appl. Mater. Interfaces* **2013**, *5*, 5954−5960.
(29) Faber, M. S.; Park, K.; Cabán-Acevedo, M.; Santra, P. K.; Jin, S. Earth-Abundant Cobalt Pyrite (CoS_2) Thin Film on Glass as a Robust, High-Performance Counter Electrode for Quantum Dot-Sensitized Solar Cells. *J. Phys. Chem. Lett.* **2013**, *4*, 1843−1849.
(30) Choi, H. M.; Ji, I. A.; Bang, J. H. Metal Selenides as a New Class of Electrocatalysts for Quantum Dot-Sensitized Solar Cells: A Tale of $Cu_{1.8}Se$ and PbSe. *ACS Appl. Mater. Interfaces* **2014**, *6*, 2335−2343.
(31) Seol, M.; Youn, D. H.; Kim, J. Y.; Jang, J.-W.; Choi, M.; Lee, J. S.; Yong, K. Mo-Compound/CNT-Graphene Composites as Efficient Catalytic Electrodes for Quantum-Dot-Sensitized Solar Cells. *Adv. Energy Mater.* **2014**, *4*, 1300775.
(32) Xiao, J.; Zeng, X.; Chen, W.; Xiao, F.; Wang, S. High Electrocatalytic Activity of Self-Standing Hollow $NiCo_2S_4$ Single Crystalline Nanorod Arrays towards Sulfide Redox Shuttles in Quantum Dot-Sensitized Solar Cells. *Chem. Commun.* **2013**, *49*, 11734−11736.
(33) Tachan, Z.; Shalom, M.; Hod, I.; Rühle, S.; Tirosh, S.; Zaban, A. PbS as a Highly Catalytic Counter Electrode for Polysulfide-Based Quantum Dot Solar Cells. *J. Phys. Chem. C* **2011**, *115*, 6162−6166.
(34) Xu, J.; Yang, X.; Wong, T.-L.; Lee, C.-S. Large-Scale Synthesis of Cu_2SnS_3 and $Cu_{1.8}S$ Hierarchical Microspheres as Efficient Counter Electrode Materials for Quantum Dot Sensitized Solar Cells. *Nanoscale* **2012**, *4*, 6537−6542.
(35) Yang, Z.; Chen, C.-Y.; Liu, C.-W.; Li, C.-L.; Chang, H.-T. Quantum Dot−Sensitized Solar Cells Featuring CuS/CoS Electrodes Provide 4.1% Efficiency. *Adv. Energy Mater.* **2011**, *1*, 259−264.
(36) Xu, J.; Yang, X.; Yang, Q.-D.; Wong, T.-L.; Lee, C.-S. Cu_2ZnSnS_4 Hierarchical Microspheres as an Effective Counter Electrode Material for Quantum Dot Sensitized Solar Cells. *J. Phys. Chem. C* **2012**, *116*, 19718−19723.
(37) Zeng, X.; Xiong, D.; Zhang, W.; Ming, L.; Xu, Z.; Huang, Z.; Wang, M.; Chen, W.; Cheng, Y.-B. Spray Deposition of Water-Soluble Multiwall Carbon Nanotube and $Cu_2ZnSnSe_4$ Nanoparticle Composites as Highly Efficient Counter Electrodes in A Quantum Dot-Sensitized Solar Cell System. *Nanoscale* **2013**, *5*, 6992−6998.
(38) Chen, H.; Zhu, L.; Liu, H.; Li, W. ITO Porous Film-Supported Metal Sulfide Counter Electrodes for High-Performance Quantum-Dot-Sensitized Solar Cells. *J. Phys. Chem. C* **2013**, *117*, 3739−3746.
(39) Lin, C.-Y.; Teng, C.-Y.; Li, T.-L.; Lee, Y.-L.; Teng, H. Photoactive p-Type PbS as a Counter Electrode for Quantum Dot-Sensitized Solar Cells. *J. Mater. Chem. A* **2013**, *1*, 1155−1162.
(40) Jiang, Y.; Zhang, X.; Ge, Q.-Q.; Yu, B.-B.; Zou, Y.-G.; Jiang, W.-J.; Hu, J.-S.; Song, W.-G.; Wan, L.-J. Engineering the Interfaces of ITO@Cu_2S Nanowire Arrays toward Efficient and Stable Counter Electrodes for Quantum-Dot-Sensitized Solar Cells. *ACS Appl. Mater. Interfaces* **2014**, *6*, 15448−15455.
(41) Yu, H.; Bao, H.; Zhao, K.; Du, Z.; Zhang, H.; Zhong, X. Topotactically Grown Bismuth Sulfide Network Film on Substrate as Low-Cost Counter Electrodes for Quantum Dot-Sensitized Solar Cells. *J. Phys. Chem. C* **2014**, *118*, 16602−16610.
(42) Li, L.; Zhu, P.; Peng, S.; Srinivasan, M.; Yan, Q.; Nair, A. S.; Liu, B.; Samakrishna, S. Controlled Growth of CuS on Electrospun Carbon Nanofibers as an Efficient Counter Electrode for Quantum Dot-Sensitized Solar Cells. *J. Phys. Chem. C* **2014**, *118*, 16526−16535.
(43) Chen, H.; Zhu, L.; Liu, H.; Li, W. Efficient Iron Sulfide Counter Electrode for Quantum Dots-Sensitized Solar Cells. *J. Power Sources* **2014**, *245*, 406−410.
(44) Hodes, G.; Manassen, J.; Cahen, D. Electrocatalytic Electrodes for the Polysulfide Redox System. *J. Electrochem. Soc.* **1980**, *127*, 544−549.
(45) Shen, C.; Sun, L.; Koh, Z. Y.; Wang, Q. Cuprous Sulfide Counter Electrodes Prepared by Ion Exchange for High-Efficiency Quantum Dot-Sensitized Solar Cells. *J. Mater. Chem. A* **2014**, *2*, 2807−2813.
(46) Jiang, Y.; Zhang, X.; Ge, Q.-Q.; Yu, B.-B.; Zou, Y.-G.; Jiang, W.-J.; Song, W.-G.; Wan, L.-J.; Hu, J.-S. ITO@Cu_2S Tunnel Junction

Nanowire Arrays as Efficient Counter Electrode for Quantum-Dot-Sensitized Solar Cells. *Nano Lett.* **2013**, *14*, 365−372.
(47) Zhao, K.; Yu, H.; Zhang, H.; Zhong, X. Electroplating Cuprous Sulfide Counter Electrode for High-Efficiency Long-Term Stability Quantum Dot Sensitized Solar Cells. *J. Phys. Chem. C* **2014**, *118*, 5683−5690.
(48) Radich, J. G.; Dwyer, R.; Kamat, P. V. Cu_2S Reduced Graphene Oxide Composite for High-Efficiency Quantum Dot Solar Cells. Overcoming the Redox Limitations of S^{2-}/S_n^{2-} at the Counter Electrode. *J. Phys. Chem. Lett.* **2011**, *2*, 2453−2460.
(49) Kumar, P.; Nagarajan, R. An Elegant Room Temperature Procedure for the Precise Control of Composition in the Cu−S System. *Inorg. Chem.* **2011**, *50*, 9204−9206.
(50) Zhao, Y.; Pan, H.; Lou, Y.; Qiu, X.; Zhu, J.; Burda, C. Plasmonic $Cu_{2-x}S$ Nanocrystals: Optical and Structural Properties of Copper-Deficient Copper(I) Sulfides. *J. Am. Chem. Soc.* **2009**, *131*, 4253−4261.
(51) Grozdanov, I.; Najdoski, M. Optical and Electrical Properties of Copper Sulfide Films of Variable Composition. *J. Solid State Chem.* **1995**, *114*, 469−475.
(52) Gadave, K. M.; Lokhande, C. D. Formation of Cu_xS Films through a Chemical Bath Deposition Process. *Thin Solid Films* **1993**, *229*, 1−4.
(53) Zhang, D.-F.; Zhang, H.; Shang, Y.; Guo, L. Stoichiometry-Controlled Fabrication of Cu_xS Hollow Structures With Cu_2O as Sacrificial Templates. *Cryst. Growth Des.* **2011**, *11*, 3748−3753.
(54) Lukashev, P.; Lambrecht, W. R. L.; Kotani, T.; van Schilfgaarde, M. Electronic and Crystal Structure of $Cu_{2-x}S$: Full-Potential Electronic Structure Calculations. *Phys. Rev. B* **2007**, *76*, No. 195202.
(55) Jiang, X.; Xie, Y.; Lu, J.; He, W.; Zhu, L.; Qian, Y. Preparation and Phase Transformation of Nanocrystalline Copper Sulfides (Cu_9S_8, Cu_7S_4, and CuS) at Low Temperature. *J. Mater. Chem.* **2000**, *10*, 2193−2196.
(56) Saldanha, P. L.; Brescia, R.; Prato, M.; Li, H.; Povia, M.; Manna, L.; Lesnyak, V. Generalized One-Pot Synthesis of Copper Sulfide, Selenide−Sulfide, and Telluride−Sulfide Nanoparticles. *Chem. Mater.* **2014**, *26*, 1442−1449.
(57) Nakai, I.; Sugitani, Y.; Nagashima, K.; Niwa, Y. X-Ray Photoelectron Spectroscopic Study of Copper Minerals. *J. Inorg. Nucl. Chem.* **1978**, *40*, 789−791.
(58) Kumar, P.; Nagarajan, R.; Sarangi, R. Quantitative X-ray Absorption and Emission Spectroscopies: Electronic Structure Elucidation of Cu_2S and CuS. *J. Mater. Chem. C* **2013**, *1*, 2448−2454.
(59) Bucur, R. V.; Berger, R. Electrochemical Potentiometric Determination of the Diffusion Coefficient of Copper in Low Digenite, A Copper Sulfide. *Solid State Ionics* **1995**, *76*, 291−296.
(60) Krylova, V.; Andrulevicius, M. Optical, XPS, and XRD Studies of Semiconducting Copper Sulfide Layers on a Polyamide Film. *Int. J. Photoenergy* **2009**, No. 304308.
(61) Xie, Y.; Riedinger, A.; Prato, M.; Casu, A.; Genovese, A.; Guardia, P.; Sottini, S.; Sangregorio, C.; Miszta, K.; Ghosh, S.; Pellegrino, T.; Manna, L. Copper Sulfide Nanocrystals with Tunable Composition by Reduction of Covellite Nanocrystals with Cu^+ Ions. *J. Am. Chem. Soc.* **2013**, *135*, 17630−17637.
(62) Hauch, A.; Georg, A. Diffusion in the Electrolyte and Charge-Transfer Reaction at the Platinum Electrode in Dye-Sensitized Solar Cells. *Electrochim. Acta* **2001**, *46*, 3457−3466.
(63) Meng, K.; Surolia, P. K.; Byrne, O.; Thampi, K. R. Efficient CdS Quantum Dot Sensitized Solar Cells Made Using Novel Cu_2S Counter Electrode. *J. Power Sources* **2014**, *248*, 218−223.
(64) Yamamoto, T.; Tanaka, K.; Kubota, E.; Osakada, K. Deposition of Copper Sulfide on the Surface of Poly(Ethylene-Terephthalate) and Poly(Vinyl Alcohol) Films in the Aqueous-Solution to Give Electrically Conductive Films. *Chem. Mater.* **1993**, *5*, 1352−1357.
(65) Murakami, T. N.; Ito, S.; Wang, Q.; Nazeeruddin, M. K.; Bessho, T.; Cesar, I.; Liska, P.; Humphry-Baker, R.; Comte, P.; Péchy, P.; Grätzel, M. Highly Efficient Dye-Sensitized Solar Cells Based on Carbon Black Counter Electrodes. *J. Electrochem. Soc.* **2006**, *153*, A2255−A2261.